nature chemical biology

ARTICLE

PUBLISHED ONLINE: 13 MARCH 2017 | DOI: 10.1038/NCHEMBIO.2334

In silico design of novel probes for the atypical opioid receptor MRGPRX2

Katherine Lansu[1,8], Joel Karpiak[2,8], Jing Liu[3], Xi-Ping Huang[1,4], John D McCorvy[1], Wesley K Kroeze[1], Tao Che[1], Hiroshi Nagase[5], Frank I Carroll[6], Jian Jin[3], Brian K Shoichet[2] & Bryan L Roth[1,4,7]*

The primate-exclusive MRGPRX2 G protein-coupled receptor (GPCR) has been suggested to modulate pain and itch. Despite putative peptide and small-molecule MRGPRX2 agonists, selective nanomolar-potency probes have not yet been reported. To identify a MRGPRX2 probe, we first screened 5,695 small molecules and found that many opioid compounds activated MRGPRX2, including (−)- and (+)-morphine, hydrocodone, sinomenine, dextromethorphan, and the prodynorphin-derived peptides dynorphin A, dynorphin B, and α- and β-neoendorphin. We used these to select for mutagenesis-validated homology models and docked almost 4 million small molecules. From this docking, we predicted ZINC-3573—a potent MRGPRX2-selective agonist, showing little activity against 315 other GPCRs and 97 representative kinases—along with an essentially inactive enantiomer. ZINC-3573 activates endogenous MRGPRX2 in a human mast cell line, inducing degranulation and calcium release. MRGPRX2 is a unique atypical opioid-like receptor important for modulating mast cell degranulation, which can now be specifically modulated with ZINC-3573.

G protein-coupled receptors (GPCRs) are seven-transmembrane receptors that transduce extracellular signals into biological responses via heterotrimeric G proteins and β-arrestins[1]. GPCRs are involved in nearly every known biological system, and, unsurprisingly, GPCR-targeting small molecules represent the largest target class of drugs approved by the US Food and Drug Administration (FDA)[2]. Despite their therapeutic utility, only 10% of GPCRs function as therapeutic targets for FDA-approved drugs[2], while ~120 of 394 nonolfactory GPCRs represent 'orphan receptors', or understudied GPCRs ("oGPCRs"[3]), for which there are no useful probes and, frequently, no validated endogenous ligands[4,5]. The process of discovering specific and potent probes for oGPCRs yields useful research tools and can illuminate previously unrealized drug interactions, potentially establishing new drug targets.

To identify oGPCR ligands, we have developed and tested new physical and computational approaches for screening these receptors. The first physical method, dubbed "PRESTO-Tango," involves high-throughput, massively parallel screening of potential modulators (including small molecules, bioactive peptides, and other reagents) for their ability to stimulate β-arrestin recruitment at most nonolfactory receptors in the GPCRome[6]. The second, an orthogonal and complementary approach, relies on the principle that overexpressed G proteins facilitate a partially active state for most GPCRs, enabling the discovery of both allosteric and orthosteric modulators for oGPCRs using engineered yeast[3]. Encouraged by the success of other structure-based drug-design methods in GPCRs[7–9], we designed an *in silico* approach that leverages the physical screens to develop comparative structural models of the receptors and then computationally screens a much wider chemical space—typically several million commercially available molecules—to find specific ligands for the oGPCRs.

We apply this strategy to the Mas-related G protein-coupled receptor X2 (MRGPRX2), a primate-exclusive[10,11] class A orphan GPCR expressed in mast cells and small-diameter neurons in the dorsal-root and trigeminal ganglia[12–16]. Several unrelated peptides are reported to activate MRGPRX2, including cortistatin-14 (ref. 16), substance P[13], and PAMP(9–20) (ref. 14); whether any proposed peptides are endogenous MRGPRX2 agonists is unknown. MRGPRX2 remains an oGPCR in part because no convincing rodent ortholog has been validated (see Discussion) and because MRGPRX2-selective nanomolar potency probes are unavailable. Although several selective agonists are reported for MRGPRX2 (refs. 17,18), the compounds are not easily obtained and have not been validated for specificity or potency. The identification of demonstrably selective, potent MRGPRX2 agonist probes represents an essential step toward illumination of its function *in vitro* and *in vivo*.

Here, we describe how an integrated approach combining our PRESTO-Tango method and our modeling and docking platforms led to the identification of MRGPRX2 agonists, including exogenous and endogenous opioids and a selective MRGPRX2 probe, ZINC-3573. We confirmed ZINC-3573's selectivity for MRGPRX2 via testing of 315 class A GPCRs using PRESTO-Tango, binding assays performed by the National Institute of Mental Health Psychoactive Drug Screening Program (NIMH-PDSP), and testing of the parent scaffold using a commercial (DiscoveRX) kinome screen. Using ZINC-3573, we showed that MRGPRX2 activation induces intracellular calcium release and degranulation in a human mast cell line. We also demonstrated that MRGPRX2 represents a novel $G\alpha_q$-coupled opioid-like receptor that could mediate some peripheral side effects of commonly prescribed opiate medications. This discovery of the specific MRGPRX2 agonist ZINC-3573, matched with an inactive enantiomer, provides the community

[1]Department of Pharmacology, University of North Carolina, Chapel Hill, North Carolina, USA. [2]Department of Pharmaceutical Chemistry, University of California, San Francisco, San Francisco, California, USA. [3]Department of Pharmacological Sciences and Department of Oncological Sciences, Icahn School of Medicine at Mount Sinai, New York, New York, USA. [4]National Institute of Mental Health Psychoactive Drug Screening Program (NIMH PDSP), University of North Carolina, Chapel Hill, North Carolina, USA. [5]International Institute for Integrative Sleep Medicine, University of Tsukuba, Tsukuba, Japan. [6]Center for Drug Discovery, Research Triangle Institute International, Research Triangle Park, North Carolina, USA. [7]Division of Chemical Biology and Medicinal Chemistry, Eshelman School of Pharmacy, University of North Carolina at Chapel Hill, Chapel Hill, North Carolina, USA. [8]These authors contributed equally to this work. *e-mail: bryan_roth@med.unc.edu

with a pair of chemical probes by which the *in vivo* function of this fascinating target may be investigated with exquisite specificity and control.

RESULTS

Identification of MRGPRX2 agonists

We initially attempted to replicate prior reports of potential MRGPRX2 agonists to determine whether any might prove suitable as leads for probe development. Unfortunately, we could not replicate the activities of most reported MRGPRX2 agonists when tested even at the highest concentrations possible for our assays (**Fig. 1**; **Supplementary Results**, **Supplementary Table 1**). Thus, of the many putative MRGPRX2-activating peptides and peptide-like compounds, we could replicate activities only for substance P, cortistatin-14, and PAMP(9-20) (**Fig. 1a**,**b**). Mastoparan, octreotide, leuprolide, and kallidin were inactive or only marginally active (for example, $G\alpha_q$ effector concentration for half-maximal response (EC_{50}) = 11.5 μM for kallidin) at human MRGPRX2 (**Fig. 1c**; **Supplementary Table 1**). The putative MRGPRX2 agonist mastoparan[19] was active both in cells with and without MRGPRX2 expression, suggesting nonspecific activity (**Fig. 1d**; **Supplementary Table 1**).

Of the more than one dozen nonpeptide compounds reported to activate MRGPRX2, we could only replicate four (TAN-67 (ref. 20), compound 48/80 (ref. 19), cetrorelix[19], and the proposed selective agonist complanadine A[18]), and even these had low potencies or have other known receptor targets (**Fig. 1c**,**d**; **Supplementary Table 1**). Notably, we could not validate several recently reported secretagogue agonists for MRGPRX2, including the THIQ-motif-containing octreotide, rocuronium, ciprofloxacin, atracurium, moxifloxacin, and levofloxacin[19], even when tested at up to 100 μM (**Fig. 1c**,**d**; **Supplementary Table 1**). Likewise, although the proposed nanomolar MRGPRX2-selective agonist complanadine A[18] was active in our assays, we measured a $G\alpha_q$ EC_{50} of 18 μM and could not obtain a β-arrestin EC_{50} because of apparent cytotoxicity above 1 μM using PRESTO-Tango, a luciferase-reporter-based β-arrestin screening platform[6] (**Fig. 1c**,**d**; see **Supplementary Table 1** for a full list of validated compounds).

As MRGPRX2 is expressed only in primates, finding a rodent analog would enable the use of genetic techniques to probe for the receptor's functional roles, with the caveat that GPCRs may often be knocked down without producing phenotypes that recapitulate their roles in pharmacology. The suggested MRGPRX2 rodent ortholog MRGPRB2 (ref. 19) shares only 52% sequence identity with MRGPRX2 (**Supplementary Fig. 1a**), and we could not substantiate any proposed shared ligands except for cortistatin-14, which had high-micromolar activity at MRGPRB2 (**Fig. 1e**,**f**; **Supplementary Fig. 1b**). Thus, although there have been prior studies of MRGPRX2 and/or MRGPRB2's pharmacology, many remain insufficiently robust for facile replication, and no independent studies have emerged that replicate these prior findings.

Accordingly, we chose an unbiased approach to identify reliable MRGPRX2 probes. We recently proposed parallel screening strategies[3,6] using small libraries of drugs and drug-like compounds as fruitful initial approaches to discover active compounds at oGPCRs[6]. Here we screened 5,695 unique compounds for agonist activity at three members of the MRGPRX family (MRGPRX1, MRGPRX2, and MRGPRX4) using the PRESTO-Tango platform (see Online Methods). Our strategy was to screen against three MRGPRX family receptors in parallel to find active compounds with selectivity within the family.

The screening revealed MRGPRX1 had the smallest number of activating compounds (39), followed by MRGPRX4 (54), and MRGPRX2 (81) (**Fig. 2a**). We were most interested in compounds showing selective MRGPRX2 agonism without apparent activity at other MRGPRX receptors. Among the 67 compounds that activated MRGPRX2 but neither MRGPRX1 nor MRGPRX4 were

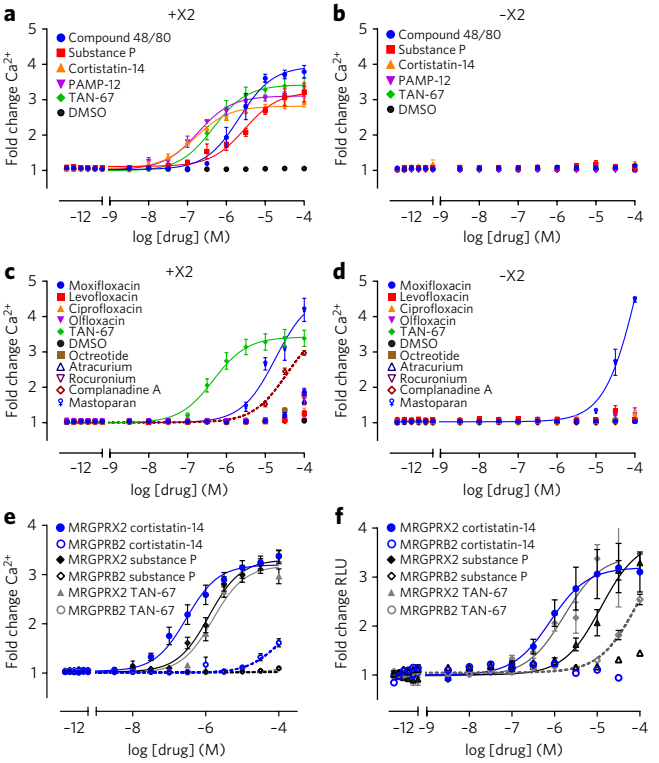

Figure 1 | Validation of MRGPRX2 and MRGPRB2 Agonists. (**a**–**d**) Average concentration–response curves in the Fluorescent imaging plate reader (FLIPR) intracellular calcium release assay (n = 3 experiments in triplicate wells) in MRGPRX2-inducible cells, designated +X2 or -X2 for the presence or absence of tetracycline-induced receptor expression, for previously published MRGPRX2 agonists. The y axis shows the fold change of calcium release over the basal receptor signaling. (**e**) Concentration–response curves in FLIPR intracellular calcium release assay for stable cell lines expressing either human MRGPRX2 (solid lines) or the proposed mouse ortholog MRGPRB2 (dotted lines) with X2-activating peptides cortistatin-14 and substance P and small-molecule agonist TAN-67. Y axis is fold-change calcium release over basal (n = 3 in quadruplicate) (**f**) Concentration–response curves for cortistatin-14, substance P, and small-molecule agonist TAN-67 with MRGPRX2-Tango (solid lines) and MRGPRB2-Tango (dotted lines) in the PRESTO-Tango arrestin recruitment assay (n = 3 in triplicate). The y axis shows the fold change response over basal luminescent signal. RLU, relative luminescent units. All error bars represent s.e.m.

five opioid-related ligands: ADL-5859, sinomenine, dextromethorphan, dextromethorphan's metabolite dextrorphan, and the previously reported MRGPRX2 ligand TAN-67 (ref. 20), a delta opioid receptor agonist.

Confirmatory concentration–response curves using the PRESTO-Tango platform indicated that the five opioid-like compounds had low-micromolar potency (**Fig. 2b**,**c**). To confirm the MRGPRX2-Tango construct performed similarly to the unmodified wild-type (WT) receptor, we tested previously reported MRGPRX2 agonists TAN-67 (ref. 20), cortistatin-14 (ref. 16), substance P[13], and compound 48/80 (ref. 19), and found that they all activated the MRGPRX2-Tango receptor at similar potencies to those reported from $G_{\alpha q}$ assays at the WT receptor (**Fig. 2d**).

To confirm MRGPRX2 $G_{\alpha q}$-mediated functional activity of agonists, we used a tetracycline-inducible WT MRGPRX2 stable HEK-T cell line to test for intracellular calcium release. Dextromethorphan, dextrorphan, sinomenine, and TAN-67 promoted intracellular calcium release when MRGPRX2 expression was induced by

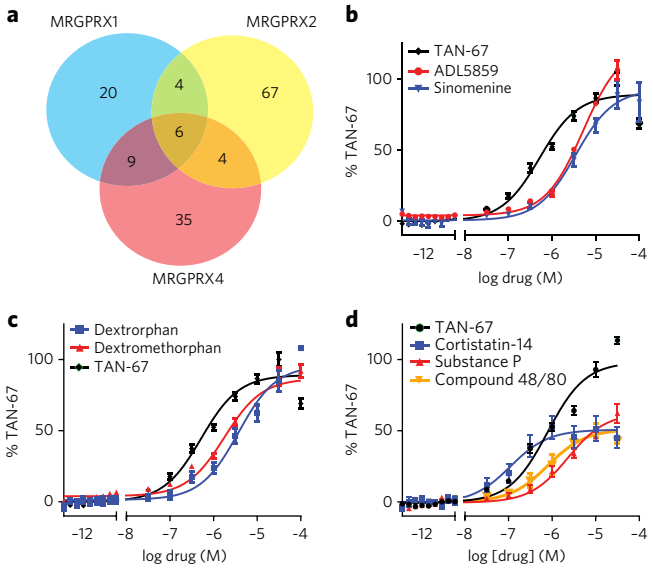

Figure 2 | PRESTO-Tango Screening of MRGPRX2 reveals new agonists. (**a**) Venn diagram depicting pooled PRESTO-Tango screening actives for MRGPRX1, MRGPRX2, and MRGPRX4 for all hits with greater than two-fold activation over basal (known false positives and duplicates excluded). (**b**,**c**) Average concentration–response curves ($n = 3$ in triplicate wells for all, except ADL5859, for which $n = 1$) for the five compounds from the screening show low micromolar activation of MRGPRX2. (**d**) Concentration–response curve for previously published MRGPRX2 peptide agonists at the MRGPRX2-Tango construct. *y* axes are shown as percent of TAN-67 activity. All error bars represent s.e.m.

tetracycline (1 μg/ml; **Supplementary Fig. 2a**) but not in the absence of tetracycline (i.e., MRGPRX2 is not expressed; **Supplementary Fig. 2b**).

Preference for dextro-enantiomers and *N*-methyl scaffolds

As several dextrorotatory opiate ligands activated MRGPRX2, we initially investigated ligand stereochemistry, aware that classical opioid receptors prefer levorotary morphinans and benzomorphans[21]. We assayed levorphanol and levallorphan, enantiomers of the screening hits dextrorphan and dextromethorphan, respectively, for activity at MRGPRX2 in β-arrestin recruitment and calcium mobilization assays. Levorphanol was approximately ten-fold less potent at MRGPRX2 than dextrorphan, and levallorphan was completely inactive up to 100 μM (**Fig. 3a**). Likewise, the dextrorotary morphinan sinomenine had comparable potency to dextrorphan and dextromethorphan at MRGPRX2 (**Supplementary Table 2**), more potent than sinomenine's purported activity at the opioid receptors[22] (**Supplementary Fig. 3**). MRGPRX2 also preferred dextrorotary benzomorphan compounds, as (−)-*cis*-normetazocine was ten-fold less potent than (+)-*cis*-normetazocine (**Fig. 3b**; **Supplementary Table 2**).

To determine whether other opioids activated MRGPRX2 with similar stereochemical preferences, we tested a panel of 11 morphine and codeine analogs for activity in PRESTO-Tango and calcium mobilization assays, including the most common metabolites of morphine and codeine. Both (+)- and (−)-morphine enantiomers activated MRGPRX2 with comparable potency in PRESTO-Tango and calcium assays, as did (+)- and (−)-codeine and thebaine (**Fig. 3c**,**d**; **Supplementary Table 2**; structures in **Fig. 3e**). For the metabolites, we observed differential effects of substitutions on C3 and C6 positions in the morphine scaffold, as replacement of morphine's 3-hydroxy with a 3-methoxy (for example, codeine and thebaine) had little effect on affinity or efficacy at MRGPRX2, whereas replacement of the morphine's 3-hydroxy with gluconuride to yield morphine-3-β-gluconuride eliminated MRGPRX2 agonist activity (**Fig. 3c**,**d**; **Supplementary Table 2**; structures in **Fig. 3e**). In the C6 position, gluconuride or acetyl modifications to morphine and codeine all retained agonist activity, albeit with loss in potency compared to (−)-morphine and (−)-codeine, respectively (**Fig. 3c**,**d**; **Supplementary Table 2**). These preliminary opioid structure–activity relationships (SAR) demonstrate that larger modifications on C6 are more tolerated than those on C3.

We then explored the effect of substituents on the cationic nitrogen in the morphinans on MRGPRX2 activation. *N*-methyl-substituted scaffolds, as in codeine, morphine, and metazocine, conferred receptor agonism while the *N*-unsubstituted-norcodeine was inactive up to 100 μM (**Fig. 3b–d**; **Supplementary Table 2**). Morphinans and benzomorphans with substituents larger than *N*-methyl, such as the *N*-allyl of levallorphan and *N*-allylnormetazocine, and the *N*-cyclopropyl of naltrexone and cyclazocine, were inactive at MRGPRX2 (**Fig. 3a**,**b**; **Supplementary Table 2**). The inactive morphinans and benzomorphans showed no antagonist activity against MRGPRX2, suggesting a tight SAR around substitution of this position.

As previously mentioned, TAN-67 is a δ-opioid receptor agonist known to activate MRGPRX2 (ref. 20). The active enantiomer at the δ-opioid receptor is (−)-TAN-67 as (+)-TAN-67 displays pronociceptive activity *in vivo* through an unidentified receptor[23]. We tested (+)-TAN-67 for MRGPRX2 activity in PRESTO-Tango and calcium mobilization assays and found that (+)-TAN-67 was more potent than racemic (+/−)-TAN-67 ($G\alpha_q$ EC_{50} = 290 nM vs. 740 nM, respectively) (**Supplementary Fig. 4**), demonstrating that MRGPRX2 prefers dextro-enantiomers at most chemical scaffolds, with some exceptions. Neither (−)- nor (+)-naloxone antagonized (+/−)-TAN-67 agonist activity (**Supplementary Fig. 5a**,**b**), and no other canonical opioid antagonists, including naltrindole, naltrexone, and β-chlornaltrexamine, inhibited (+/−)-TAN-67 activity. (**Supplementary Fig. 5c–d**). These SARs suggests that MRGPRX2, despite its distant sequence relationship to the four classic opioid receptors (transmembrane region sequence identity no greater than 26%), is an opioid-responding oGPCR with important differences in ligand recognition patterns.

Prodynorphin-derived peptides activate MRGPRX2

A key question is whether MRGPRX2 is also activated by endogenous opioid ligands. Accordingly, we tested a panel of 20 endogenous opioid peptides for activity in PRESTO-Tango and intracellular calcium assays. MRGPRX2 was preferentially activated by prodynorphin-derived peptides (**Fig. 4a**,**b**) and only minimally activated, if at all, by other opioid peptides (**Fig. 4c**,**d**). The full-length dynorphin A(1–17) and several truncated prodynorphin peptides activated MRGPRX2 (**Fig. 4a**). C-terminal amino acid truncation of dynorphin peptides progressively reduced agonist potency until the dynorphin A(1–7) and dynorphin A(1–6) fragments, which were completely inactive (**Fig. 4a**; **Supplementary Fig. 6a**).

To determine whether the C-terminal portion of dynorphin A was sufficient for MRGPRX2 activation, we assayed dynorphin A(13–17) and dynorphin A(6–17) and found that dynorphin A(6–17) retained minimal activity (EC_{50} = 39.6 μM) and dynorphin A(13–17) was inactive (**Fig. 4b**), suggesting that both the N-terminal YGGF motif and C-terminal cationic tail are important for MRGPRX2 activation (**Supplementary Fig. 6a**). Dynorphin B(1–13) and α- and β-neoendorphin also activated MRGPRX2, with dynorphin B and α-neoendorphin having almost identical μM potency (**Fig. 4b**). Intriguingly, EC_{50} values for the dynorphin peptides were right-shifted in the PRESTO-Tango assay, indicating perhaps modest G protein bias, similar to observations made for dynorphin peptides at the κ-opioid receptor[24].

To determine whether more closely related receptors might share peptide ligands with MRGPRX2, we used the GPCRDB[25]

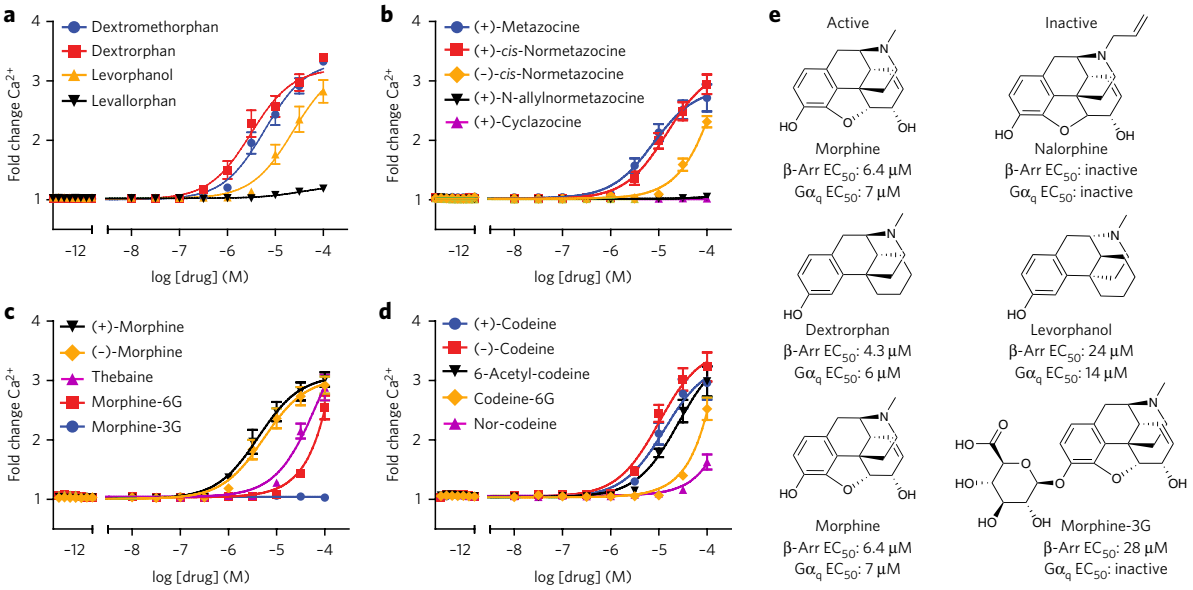

Figure 3 | MRGPRX2 is activated by many opioid scaffolds. (**a**–**d**) Average concentration–response curves (n = 3 in triplicate) for structurally related compounds, morphinans (**a**), benzomorphans (**b**), morphine and analogs (**c**), and codeine and analogs (**d**), in an intracellular calcium release assay in which the y axis is fold-change calcium release over baseline. Error bars represent s.e.m. (**e**) Summary of major findings in structure–activity relationships for opioid scaffolds at MRGPRX2, including size of N-substituent, stereochemistry of chiral centers, and bulk on the 3-position of the morphinan.

to identify class A receptors with ≥30% sequence similarity to MRGPRX2 in the class A binding pocket (**Supplementary Fig. 6b**). We identified 14 receptors, 11 of which had established probes (10 ligands total). Three receptors were oGPCRs with no known ligands. We tested the ten established ligands for activity and found that only one, somatostatin-14, activated MRGPRX2 (**Supplementary Fig. 5b**,**d**; EC_{50} = 380 nM). This result is consistent with previous reports that somatostatin-14, somatostatin-28, and cortistatin-14 are MRGPRX2 agonists[16,20]. Interestingly, the canonical opioid receptors and somatostatin receptors are closely related in binding-site-sequence space but not in small-molecule chemical space[26]. Our data, along with previously proposed peptide ligands, suggest that although MRGPRX2 can be activated by many peptide ligands, this cannot be predicted from sequence similarity alone.

MRGPRX2 is an opioid-like oGPCR that responds to endogenous pro-dynorphin-derived opioid peptides and binds to many well-known synthetic opioid agonists, but differs from classic opioid receptors in its unique preference for dextromorphinans and dextrobenzomorphans as well as its inability to be antagonized by potent and classic opioid receptor antagonists. Although none of these compounds are suitable as a selective probe or tool, the chemical matter identified was useful to launch an *in silico* campaign to identify novel chemotypes active at MRPGRX2.

Structure-based docking predicts MRGPRX2-selective ligands

We next turned to our computational approach, using a 1,000-fold larger compound library than that used in the physical screen—the over 3.7-million commercially available 'lead-like' molecules then in the ZINC database[27]. Our strategy was to calculate many 3D MRGPRX2 models, select those few that recapitulated the ligand recognition patterns we observed experimentally, and use these to create a template of a final model to screen the full, larger compound library for novel molecules unrelated to opioid ligands but selective for MRGPRX2.

The general approach for modeling and docking has been recently described[3], and we summarize it here (see Online Methods for more details). We first sought GPCRs of known structure with MRGPRX2 sequence similarity; intriguingly, this led to the κ-opioid receptor, which shares only 23.3% sequence identity in the transmembrane regions with MRGPRX2. We calculated an initial MRGPRX2 structure using Modeller[28] and expanded on this using elastic network modeling to increase the amount of sampled backbone conformations[29]. From the initial model, we calculated 360 further structures using the elastic network modeling program (ENM); half of these

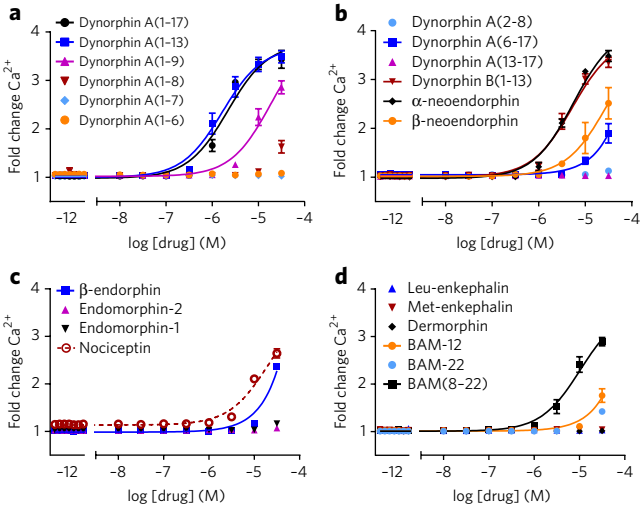

Figure 4 | MRGPRX2 is preferentially activated by prodynorphin-derived peptides. (**a**,**b**) Average concentration response curves (in triplicate wells; n = 3 for all except Dyn A fragments below 7 amino acids in length and α-neoendorphin for which n = 2 ; see **Supplementary Table 2**) for pro-dynorphin-derived peptides in MRGPRX2 Tet-On cells, in which the y axis is fold-change calcium release over baseline. Error bars represent s.e.m. (**c**,**d**) Average concentration–response curves (in triplicate wells; n = 3 for all except nociceptin and BAM(8–22) for which n = 2 and β-endorphin and BAM-22 for which n =1 ; see **Supplementary Table 2**) depicting nonprodynorphin-derived peptides with minimal activity compared to dynorphins in A and B. Error bars represent s.e.m.

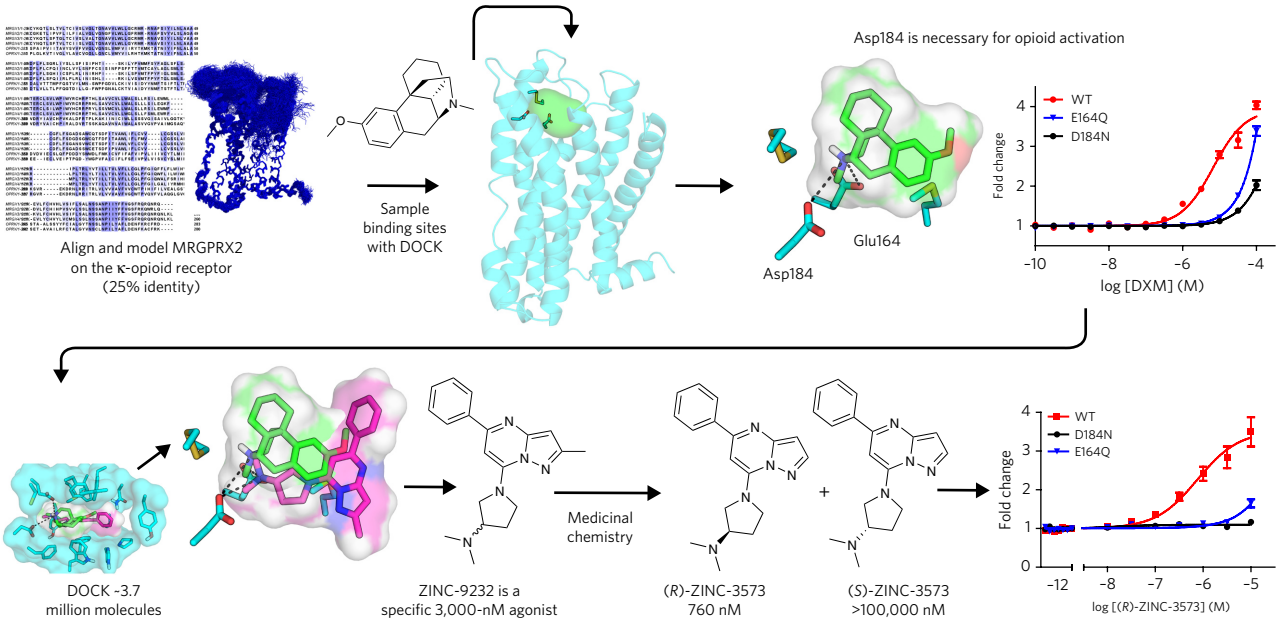

Figure 5 | *In silico* MRGPRX2 homology modeling predicts a selective agonist. Workflow depicting MRGPRX2 homology model construction (top left) followed by identification of a putative binding site (top middle) that was confirmed by testing the mutations E164Q and D184N (top right, average dose response, $n = 3$ in triplicate, shown with dextromethorphan (DXM). Then, ~3.7 million molecules were docked to predict the agonist ZINC-9232 (bottom left). Further iteration and testing revealed the tool and selective compounds (*S*)- and (*R*)-ZINC-3573 (bottom middle and right). Docking pose of selective compound is supported with mutation experiments in PRESTO-Tango (bottom right, average dose–response curve, average of $n = 4$ in triplicate). Error bars on graphs shown is representative of s.e.m.

structures had an extracellular disulfide bond imposed and half did not. Each of these was expanded three-fold with Modeller (i.e., using the ENM models as templates for Modeller). Overall, 1,080 models were calculated.

We docked the 5,695 unique compounds from the physical screening against all 1,080 models (i.e., over 6 million compound–receptor docking calculations, and over 10^{12} individual configurations of the library molecules in the receptor). We looked for models that best enriched the discovered opioid agonists over the vast number of inactive decoy molecules. The top-enriching models were inspected visually for binding poses that captured sensible ion-pairing interactions with the conserved aminergic group of the opioid agonists. This prioritized a model that had a background-corrected area under the receiver operating characteristic curve (logAUC), for enrichment[30,31] of 8.42—which happened to be the top-enriching model (this is not always the case, as sometimes the top-enriching model does not have sensible geometries[32], though usually the model chosen is among the best enriching models). Residues within 6 Å of the dextromethorphan pose were minimized around the docked ligand with protein local optimization program (PLOP)[33] and the 5,695 molecules redocked. Two rounds of docking and PLOP-based refinement led to the final modeled receptor conformation, which predicts the opioid agonists making ionic interactions with Glu164$^{4.60}$ and Asp184$^{5.38}$ (**Fig. 5**, showing dextromethorphan); superscripts indicate Ballesteros–Weinstein residue numbering[34] based our MGPRX2 alignment with κ-opioid receptor (**Supplementary Fig. 6c**). The exact rotamer state of these residues allowed some flexibility; i.e., several different rotamers of the Asp and Glu led to productive placement of the known agonists (**Supplementary Fig. 7e**).

To test the predicted ion pair between the receptor and the ligands, we made a series of mutations at Glu164$^{4.60}$ and Asp184$^{5.38}$. E164Q and D184N substitutions retained steric properties of the WT residues but removed their negative charges, and both resulted in a loss of activity for dextromethorphan, (−)-morphine, and related opioids in the PRESTO-Tango assay (**Fig. 5**; **Supplementary Fig. 7a**). We then tested the importance of the length of the acidic residue via E164D and D184E mutations and observed that E164D increased the efficacy and reduced the potency of both dextrorphan and morphine (**Supplementary Fig. 7a**,**c**) whereas D184E ablated activity of all opioids tested (**Fig. 5**; **Supplementary Fig. 7a–d**). The substitutions support the importance of the proposed ionic interaction and the putative binding site predicted by the *in silico* model, suggesting both Glu164$^{4.60}$ and Asp184$^{5.38}$ are necessary for MRGPRX2 opioid activation.

As an aside, dynorphin A(1–13) activity was lost with the D184N but not the E164Q mutation, suggesting that only one of these residues is required for the opioid–peptide interaction (**Supplementary Fig. 7d**). We modeled the putative MRGPRX2–dynorphin binding site by overlaying the MRGPRX2 homology model with the previously published κ-opioid receptor docked with dynorphin A(1–13)[35]. The N-terminal Tyr1 of dynorphin A(1–13) is accommodated within a negatively charged aromatic pocket, whereas Arg7 and Phe4 appear to interact with Asp184$^{5.38}$ (**Supplementary Fig. 8a–c**). The predicted orientation of dynorphin A(1–13) at Asp184$^{5.38}$ and Glu164$^{4.60}$ shows a clear preference for charged interactions between dynorphin A and Asp184$^{5.38}$, an outcome supported by the mutagenesis results (**Supplementary Fig. 8d**).

With experimental support for the MRGPRX2 comparative model, we proceeded to virtually screen the ZINC library for new ligands. Over 3.7 million commercially available molecules were docked, each in an average of 926 orientations and 558 conformations; overall, 1.9 trillion docked complexes were sampled and scored (for details, see Online Methods). We selected, purchased, and assayed 20 compounds from the 0.13% of top-ranked compounds for activity at MRGPRX2. As there is little scoring difference among the top-ranked molecules, we chose molecules following our usual strategy[36] and prioritized those with diverse, nonopioid chemotypes. We deprioritized molecules with apparently high internal energies, which the docking scoring function does not well account

for[36], and prioritized those that made ionic interactions with the Asp184$^{5.38}$ and Glu164$^{4.60}$ pair, similarly to the modeled opioids. Of the 20 ZINC compounds tested, one, ZINC-72469232 (**1**, here on referred to as ZINC-9232), had substantial activity below 10 μM in PRESTO-Tango and calcium release assays (**Fig. 5**). To improve potency, 22 analogs of ZINC-9232 topologically similar to the lead were obtained and tested. Of these 22, seven were active, with the most potent being ZINC-72453573 (**2**, from here on referred to as ZINC-3573), having submicromolar potency (EC_{50} = 760 nM, **Fig. 5**; **Supplementary Fig. 9**). We then assessed whether ZINC-3573 interacts with the predicted residues Asp184$^{5.38}$ and Glu164$^{4.60}$ using the E164Q and D184N mutations and found that both eliminated ZINC-3573 agonism at MRGPRX2 (**Fig. 5**), consistent with the modeling.

ZINC-3573 as a chemical probe for MRGPRX2

To confirm MRGPRX2 selectivity, we tested ZINC-9232 and ZINC-3573 activity at 315 other human GPCRs using our PRESTO-Tango GPCRome assay. ZINC-9232 and ZINC-3573 showed minimal agonist efficacy at receptors other than MRGPRX2 at 10 μM (**Supplementary Fig. 10a**,**b**). ZINC-9232 was also screened against a panel of 97 representative human kinases using the DiscoveRX KINOMEscan diversity panel; only three kinases were modestly inhibited, with IC_{50} values between 20–30 μM (**Supplementary Fig. 11**).

These results encouraged us to synthesize both enantiomers of the more potent ZINC-3573, originally supplied as a racemic mixture, in an effort to create a pair of differentially active molecules that could be used jointly as a chemical probe pair (**Supplementary Note**). The *R*-isomer (**3**) retained an EC_{50} of 740 nM in PRESTO-Tango and a similar EC_{50} value of 1 μM in the calcium mobilization assay (**Supplementary Fig. 9**). The *S*-isomer (**4**) had little activity below concentrations of 100 μM (**Supplementary Fig. 9**). The separate activity of the enantiomers makes them highly attractive probes, as one can distinguish MRGPRX2 activity (owing to the *R*-isomer) from general, nonspecific activity because of the scaffold and its physical properties (due to either isomer's attributes). Each enantiomer was further tested using the PRESTO-Tango GPCRome screening platform (**Supplementary Fig. 10c**,**d**), which indicated that 21 receptors may be activated two-fold or more with (*R*)- and (*S*)-ZINC-3573; however, subsequent concentration–response studies showed that no other receptor was substantially activated by either compound (**Supplementary Fig. 11**).

MRGPRX2 agonists induce degranulation in mast cells

MRGPRX2 has been implicated in IgE-independent inflammatory responses in mast cells using peptide ligands and other nonspecific agonists[13,15,19], prompting us to investigate whether MRGPRX2-selective agonists induce degranulation and mobilize intracellular calcium in the LAD2 human mast cell line. ZINC-9232 and ZINC-3573 induced intracellular calcium release and degranulation in LAD2 mast cells at comparable potencies to calcium and β-arrestin assays performed in MRGPRX2-expressing HEK-T cells (**Fig. 6a**,**b**). For the stereochemical pair, only (*R*)-ZINC-3573 promoted degranulation in LAD2 mast cells (**Fig. 6b**), consistent with the HEK-T *in vitro* activity. As expected, MRGPRX2 siRNA (short interfering RNA) significantly reduced (*R*/*S*)-ZINC-3573-induced degranulation (**Fig. 6c**; $P = 0.01$).

We then considered whether the opioid ligands might activate endogenously expressed MRGPRX2 to induce degranulation in mast cells. This is important, in part, because of the well-known but enigmatic 'histamine flush' associated with many opioids, which is not due to engagement of classical opioid receptors. We found that (+/−)-TAN-67, (+)-morphine, (−)-morphine, and dynorphin A(1–13) produced robust intracellular calcium release in the mast cells, while the structurally similar κ-opioid receptor agonist

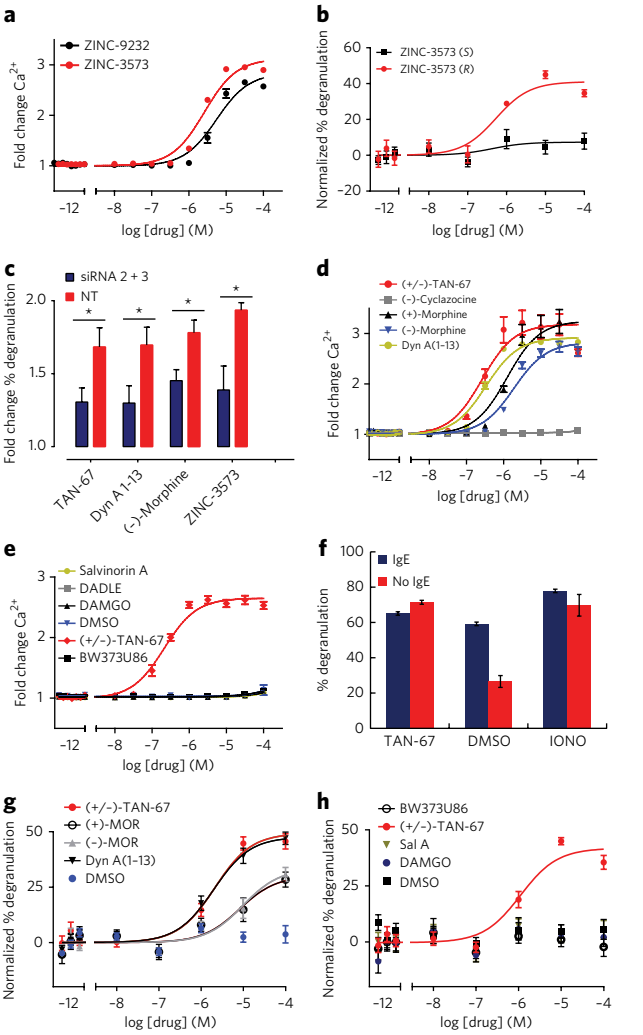

Figure 6 | MRGPRX2 mediates intracellular calcium release and degranulation in the LAD2 human mast cell line. (**a**) Average concentration response for MRGPRX2-selective agonists ZINC-9232 and ZINC-3573 in the calcium mobilization assay in LAD2 mast cells ($n = 3$ in triplicate). (**b**) Average concentration response ($n = 3$ in triplicate) for MRGPRX2 probes ZINC-3573 (*R*) and ZINC-3573 (*S*) in the β-hexosaminidase degranulation assay in LAD2 cells. (**c**). Bar graph depicting fold change percent degranulation (baseline is average DMSO of all plates) induced by EC_{80} concentration of drug following 25 nM MRGPRX2 siRNA transfection. NT, non-targeting pool; siRNA 2 + 3, MRGPRX2 siRNA pool. Statistics were calculated using two-way ANOVA with a Sidak *post hoc* test ($P < 0.05$ = *; $P = 0.031$, 0.031, 0.033, and 0.017 for TAN, dynorphin A (Dyn A), morphine, and ZINC-3573, respectively). $n = 3$ for all except ZINC-3573, for which $n = 2$. All replicates in triplicate wells. (**d**) Concentration–response curves for MRGPRX2-activating opioid ligands and the structurally related, κ-opioid receptor ligand (−)-cyclazocine in the calcium mobilization assay ($n = 3$ in triplicate). (**e**) Average concentration response in intracellular calcium release with MRGPRX2-activating (+/−)-TAN-67 and canonical opioid receptor ligands DADLE, DAMGO, salvinorin A, and BW373U86 ($n = 3$ in triplicate). (**f**) Bar graph depicting baseline normalized percent degranulation induced for each 10 μM (+/−)-TAN-67, DMSO, and calcium ionophore ionomycin (IONO) in the presence of absence of biotin-labeled IgE antibodies. (streptavidin in all wells, average of $n = 2$ in triplicate.) (**g**) Average concentration–response curves for MRGPRX2-activating opiates ($n = 3$ in triplicate) in the β-hexosaminidase degranulation assay. (**h**) Degranulation concentration response with canonical opioid receptor agonists and MRGPRX2-activating (+/−)-TAN-67, ($n = 3$ in triplicate). All error bars demonstrate s.e.m.

(−)-cyclazocine, which does not activate MRGPRX2, did not (**Fig. 6d**). Correspondingly, structurally unrelated agonists for the κ, δ, and μ opioid receptors (salvinorin A, BW373U86, and DAMGO, respectively) were inactive (**Fig. 6e**). To determine whether MRGPRX2-activating opioids induce degranulation, we first tested 10 μM (+/−)-TAN-67 in the presence or absence of biotin-labeled IgE antibodies and found that with or without IgE-biotin antibody activation via streptavidin, the MRGPRX2 ligand (+/−)-TAN-67 produced 70% degranulation, indicating that MRGPRX2-mediated degranulation is IgE-independent (**Fig. 6f**). MRGPRX2 agonists (+/−)-TAN-67, (+)-morphine, (−)-morphine, and dynorphin A(1–13) all promoted degranulation in LAD2 cells (**Fig. 6g**), while the classical opioid agonists salvinorin A, BW373U86 and DAMGO did not (**Fig. 6h**). 10 μM naloxone pretreatment did not influence the EC_{50} or efficacy of MRGPRX2 opioid agonists (**Supplementary Fig. 12a**,**b**), whereas MRGPRX2 siRNA significantly attenuated (+/−)-TAN-67-, dynorphin A(1–13)-, and (−)-morphine-induced degranulation (**Fig. 6c**; **Supplementary Fig. 12c**,**d**). These data suggest that MRGPRX2, not the canonical opioid receptors, mediates opioid-induced degranulation in human mast cells.

DISCUSSION

Our MRGPRX2 results underscore two major findings. First, the oGPCR MRGPRX2 responds to opioid drugs and endogenous pro-dynorphin peptides at potentially physiologically relevant concentrations and mediates opioid-induced degranulation in a human mast cell line. Although this receptor is not in the opioid receptor family by sequence similarity, its agonism by opioid drugs and peptides qualifies it as an atypical opioid receptor that responds to morphinan-based opioids and transmitters. A second key result is the structure-based discovery of the selective, submicromolar MRGPRX2 agonist (*R*)-ZINC-3573. This agonist promotes degranulation in mast cells and has no measurable agonism at over 315 other GPCRs, and the parent scaffold has little activity against 97 representative kinases. The inactive enantiomer (*S*)-ZINC-3573 and the active (*R*)-ZINC3573 are an effective and internally controlled probe pair for investigating the biology of this intriguing primate-exclusive receptor. The probes will be made available to the community from Sigma-Aldrich (#SML1699 and #SML1700).

SAR results show MRGPRX2 is distinct from the canonical opioid receptors. MRGPRX2 prefers dextro-enantiomers and *N*-methyl-substituted opioid scaffolds, whereas opioid receptors prefer levo-enantiomer opioids[21,37] and tolerate a wider array of *N*-substituents. In further contradistinction to the canonical opioid receptors, MRGPRX2 is $G\alpha_q$ rather than $G\alpha_i$ coupled. Thus, MRGPRX2 may be classified as an atypical opioid-recognizing receptor, arguably a better example of convergent evolution within the GPCR family than of the divergent evolution that relates the four canonical opioid receptors.

MRGPRX2 activation by opiates may be physiologically and therapeutically relevant. We found that MRGPRX2, not the canonical opioid receptors, mediates morphine and dynorphin A(1–13)-induced mast cell degranulation. Morphine and structurally similar analgesics induce mast cell histamine release[38,39] in humans, resulting in pruritus[40], vasodilation, and hypotension that is poorly reversed by naloxone[38,41]; these effects are not seen for opioid analgesics lacking MRGPRX2 activity, such as fentanyl[39]. MRGPRX2 may also be involved in the efficacy of sinomenine, which is used to treat rheumatoid arthritis because of its histamine-releasing properties[42]. Dextromethorphan's potency at MRGPRX2 is also greater than or equal to reported K_i values for μ, κ, δ, NMDA, and σ_2 receptors[21], suggesting that MRGPRX2 could contribute to dextromethorphan's side-effect profile, which includes itch at high doses[43]. Definitive studies in nonhuman primates are needed to address these hypotheses.

The micromolar potency of pro-dynorphin peptides at MRGPRX2 suggests that *in vivo* receptor activation might require them to be in close proximity to high local concentrations of dynorphin. Local synaptic concentrations of neuropeptides can reach millimolar range[44], and dynorphin is expressed in MRGPRX2-expressing regions[45–47]. At such concentrations, dynorphin could activate synaptic GPCRs or those expressed in mast cells, which can localize to nerve terminals[48]. Thus, it is conceivable that MRGPRX2 is exposed to activating concentrations of dynorphin *in vivo*.

Structural modeling enabled the discovery of a new scaffold, represented by ZINC-9232 and ZINC-3573, unrelated to classical opioids topologically and structurally. The unusual specificity of ZINC-3573 against essentially the entire GPCRome and the relevant kinome, and the availability of an inactive enantiomer, makes this molecule a uniquely useful MRGPRX2 probe. Methodologically, we previously used the combination of an initial physical compound screen followed by a much larger docking screen to discover probes for oGPCRs[3]. Identification of ZINC-3573 by a similar approach against a wholly different receptor family suggests this approach has broad utility in structure-based drug design.

The modeled MRGPRX2 provided intriguing insights to this receptor's unique opioid pharmacology. MRGPRX2 shares no more than 26% sequence identity with the μ-, κ-, δ-, or nociceptin-opioid receptors, and its modeled orthosteric binding differs from that of the canonical opioid receptors. The cationic nitrogen of the morphinans is recognized by an aspartate in the opioid receptors, located in transmembrane (TM) helix 3, position 3.32. The residue for cationic nitrogen recognition in MRGPRX2 appears instead to be in TM5, Asp184$^{5.38}$ (see **Supplementary Fig. 6c**). Many other recognition residues do not overlap in sequence or structural placement. Indeed, the entire region surrounding Asp184$^{5.38}$ and Glu164$^{4.60}$ of the MRGPRX2 putative binding site is closed off from ligand contacts in the classical opioid binding site by Tyr$^{3.33}$—a smaller Thr110 in MRGPRX2. These seeming mismatches reflect that different receptor environments can recognize related ligand chemistry and the capacity for ligands to interact with receptors from different evolutionary families[26,49] and different G protein coupling.

Certain caveats merit airing. We have not determined the structure of MRGPRX2 in complex with any of the ligands discussed here, and the modeling that we have used to interpret activity and to predict new molecules—however successfully—must remain tentative. Until the opioid actions at this receptor can be probed *in vivo*, so, too, must the physiological implications. We note that a prior study also suggested that MRGPRX2 is a novel "morphine receptor" that mediates some of morphine's analgesic activity[50]. Whereas this report certainly shares some similarity with our observations, we find, in contrast, that MRGPRX2 is more potently activated by (+)-, rather than (−)-, morphine, suggesting MRGRPX2 is unlikely to confer analgesia, as (+)-morphine is devoid of such activity[37,51].

MRGPRX2 is a novel $G\alpha_q$-coupled opioid-like receptor activated by endogenous prodynorphin-derived peptides and opioid compounds, including FDA-approved drugs and their metabolites. The discovery of selective and relatively potent MRGPRX2 agonist (*R*)-ZINC-3573 and its inactive *S*-isomer provides researchers with a chemical probe pair to specifically modulate this receptor, illuminating its role in pathological reactions such as itch and potentially revealing a path for therapeutic design.

Received 11 August 2016; accepted 22 December 2016;
published online 13 March 2017

METHODS

Methods, including statements of data availability and any associated accession codes and references, are available in the online version of the paper.

References

1. Allen, J.A. & Roth, B.L. Strategies to discover unexpected targets for drugs active at G protein-coupled receptors. *Annu. Rev. Pharmacol. Toxicol.* **51**, 117–144 (2011).
2. Overington, J.P., Al-Lazikani, B. & Hopkins, A.L. How many drug targets are there? *Nat. Rev. Drug Discov.* **5**, 993–996 (2006).
3. Huang, X.P. *et al.* Allosteric ligands for the pharmacologically dark receptors GPR68 and GPR65. *Nature* **527**, 477–483 (2015).
4. Rask-Andersen, M., Masuram, S. & Schiöth, H.B. The druggable genome: evaluation of drug targets in clinical trials suggests major shifts in molecular class and indication. *Annu. Rev. Pharmacol. Toxicol.* **54**, 9–26 (2014).
5. Fredriksson, R. & Schiöth, H.B. The repertoire of G-protein-coupled receptors in fully sequenced genomes. *Mol. Pharmacol.* **67**, 1414–1425 (2005).
6. Kroeze, W.K. *et al.* PRESTO-Tango as an open-source resource for interrogation of the druggable human GPCRome. *Nat. Struct. Mol. Biol.* **22**, 362–369 (2015).
7. Ngo, T. *et al.* Identifying ligands at orphan GPCRs: current status using structure-based approaches. *Br. J. Pharmacol.* **173**, 2934–2951 (2016).
8. Isberg, V. *et al.* Computer-aided discovery of aromatic l-α-amino acids as agonists of the orphan G protein-coupled receptor GPR139. *J. Chem. Inf. Model.* **54**, 1553–1557 (2014).
9. Mason, J.S., Bortolato, A., Congreve, M. & Marshall, F.H. New insights from structural biology into the druggability of G-protein-coupled receptors. *Trends Pharmacol. Sci.* **33**, 249–260 (2012).
10. Zylka, M.J., Dong, X., Southwell, A.L. & Anderson, D.J. Atypical expansion in mice of the sensory neuron-specific Mrg G-protein-coupled receptor family. *Proc. Natl. Acad. Sci. USA* **100**, 10043–10048 (2003).
11. Dong, X., Han, S., Zylka, M.J., Simon, M.I. & Anderson, D.J. A diverse family of GPCRs expressed in specific subsets of nociceptive sensory neurons. *Cell* **106**, 619–632 (2001).
12. Lembo, P.M. *et al.* Proenkephalin A gene products activate a new family of sensory neuron-specific GPCRs. *Nat. Neurosci.* **5**, 201–209 (2002).
13. Tatemoto, K. *et al.* Immunoglobulin E-independent activation of mast cell is mediated by Mrg receptors. *Biochem. Biophys. Res. Commun.* **349**, 1322–1328 (2006).
14. Kamohara, M. *et al.* Identification of MrgX2 as a human G-protein-coupled receptor for proadrenomedullin N-terminal peptides. *Biochem. Biophys. Res. Commun.* **330**, 1146–1152 (2005).
15. Subramanian, H. *et al.* β-Defensins activate human mast cells via Mas-related gene X2. *J. Immunol.* **191**, 345–352 (2013).
16. Robas, N., Mead, E. & Fidock, M. MrgX2 is a high potency cortistatin receptor expressed in dorsal root ganglion. *J. Biol. Chem.* **278**, 44400–44404 (2003).
17. Malik, L. *et al.* Discovery of non-peptidergic MrgX1 and MrgX2 receptor agonists and exploration of an initial SAR using solid-phase synthesis. *Bioorg. Med. Chem. Lett.* **19**, 1729–1732 (2009).
18. Johnson, T. & Siegel, D. Complanadine A, a selective agonist for the Mas-related G protein-coupled receptor X2. *Bioorg. Med. Chem. Lett.* **24**, 3512–3515 (2014).
19. McNeil, B.D. *et al.* Identification of a mast-cell-specific receptor crucial for pseudo-allergic drug reactions. *Nature* **519**, 237–241 (2015).
20. Southern, C. *et al.* Screening β-arrestin recruitment for the identification of natural ligands for orphan G-protein-coupled receptors. *J. Biomol. Screen.* **18**, 599–609 (2013).
21. Sromek, A.W. *et al.* Preliminary pharmacological evaluation of enantiomeric morphinans. *ACS Chem. Neurosci.* **5**, 93–99 (2014).
22. Wang, M.H. *et al.* Activation of opioid mu-receptor by sinomenine in cell and mice. *Neurosci. Lett.* **443**, 209–212 (2008).
23. Nagase, H. *et al.* The pharmacological profile of delta opioid receptor ligands, (+) and (−) TAN-67 on pain modulation. *Life Sci.* **68**, 2227–2231 (2001).
24. White, K.L. *et al.* Identification of novel functionally selective κ-opioid receptor scaffolds. *Mol. Pharmacol.* **85**, 83–90 (2014).
25. Horn, F. *et al.* GPCRDB: an information system for G-protein-coupled receptors. *Nucleic Acids Res.* **26**, 275–279 (1998).
26. Lin, H., Sassano, M.F., Roth, B.L. & Shoichet, B.K. A pharmacological organization of G protein-coupled receptors. *Nat. Methods* **10**, 140–146 (2013).
27. Irwin, J.J. & Shoichet, B.K. ZINC--a free database of commercially available compounds for virtual screening. *J. Chem. Inf. Model.* **45**, 177–182 (2005).
28. Eswar, N. *et al.* Comparative protein structure modeling using MODELLER. *Curr. Protoc. Protein Sci.* **50**, 2.9.1–2.9.31 (2007).
29. Yang, Q. & Sharp, K.A. Building alternate protein structures using the elastic network model. *Proteins* **74**, 682–700 (2009).
30. Mysinger, M.M. & Shoichet, B.K. Rapid context-dependent ligand desolvation in molecular docking. *J. Chem. Inf. Model.* **50**, 1561–1573 (2010).
31. Mysinger, M.M. *et al.* Structure-based ligand discovery for the protein–protein interface of chemokine receptor CXCR4. *Proc. Natl. Acad. Sci. USA* **109**, 5517–5522 (2012).
32. Carlsson, J. *et al.* Ligand discovery from a dopamine D3 receptor homology model and crystal structure. *Nat. Chem. Biol.* **7**, 769–778 (2011).
33. Jacobson, M.P., Friesner, R.A., Xiang, Z. & Honig, B. On the role of the crystal environment in determining protein side chain conformations. *J. Mol. Biol.* **320**, 597–608 (2002).
34. Ballesteros, J.A. & Weinstein, H. Integrated methods for the construction of three-dimensional models and computational probing of structure–function relations in G-protein-coupled receptors. *Methods Neurosci.* **25**, 366–428 (1995).
35. O'Connor, C. *et al.* NMR structure and dynamics of the agonist dynorphin peptide bound to the human kappa opioid receptor. *Proc. Natl. Acad. Sci. USA* **112**, 11852–11857 (2015).
36. Irwin, J.J. & Shoichet, B.K. Docking screens for novel ligands conferring new biology. *J. Med. Chem.* **59**, 4103–4120 (2016).
37. Jacquet, Y.F., Klee, W.A., Rice, K.C., Iijima, I. & Minamikawa, J. Stereospecific and nonstereospecific effects of (+)- and (−)-morphine: evidence for a new class of receptors? *Science* **198**, 842–845 (1977).
38. Baldo, B.A. & Pham, N.H. Histamine-releasing and allergenic properties of opioid analgesic drugs: resolving the two. *Anaesth. Intensive Care* **40**, 216–235 (2012).
39. Rosow, C.E., Moss, J., Philbin, D.M. & Savarese, J.J. Histamine release during morphine and fentanyl anesthesia. *Anesthesiology* **56**, 93–96 (1982).
40. Kumar, K. & Singh, S.I. Neuraxial opioid-induced pruritus: an update. *J. Anaesthesiol. Clin. Pharmacol.* **29**, 303–307 (2013).
41. Hutchinson, M.R. *et al.* Exploring the neuroimmunopharmacology of opioids: an integrative review of mechanisms of central immune signaling and their implications for opioid analgesia. *Pharmacol. Rev.* **63**, 772–810 (2011).
42. Yamasaki, H. Pharmacology of sinomenine, an anti-rheumatic alkaloid from *Sinomenium acutum*. *Acta Med. Okayama* **30**, 1–20 (1976).
43. Zajac, M. *et al.* [Recreational usage of dextromethorphan—analysis based on internet users experiences]. *Przegl. Lek.* **70**, 525–527 (2013).
44. Scimemi, A. & Beato, M. Determining the neurotransmitter concentration profile at active synapses. *Mol. Neurobiol.* **40**, 289–306 (2009).
45. Podvin, S., Yaksh, T. & Hook, V. The emerging role of spinal dynorphin in chronic pain: a therapeutic perspective. *Annu. Rev. Pharmacol. Toxicol.* **56**, 511–533 (2016).
46. Sweetnam, P.M., Neale, J.H., Barker, J.L. & Goldstein, A. Localization of immunoreactive dynorphin in neurons cultured from spinal cord and dorsal root ganglia. *Proc. Natl. Acad. Sci. USA* **79**, 6742–6746 (1982).
47. Rojewska, E., Makuch, W., Przewlocka, B. & Mika, J. Minocycline prevents dynorphin-induced neurotoxicity during neuropathic pain in rats. *Neuropharmacology* **86**, 301–310 (2014).
48. Bienenstock, J. *et al.* Mast cell/nerve interactions in vitro and in vivo. *Am. Rev. Respir. Dis.* **143**, S55–S58 (1991).
49. Barelier, S., Sterling, T., O'Meara, M.J. & Shoichet, B.K. The recognition of identical ligands by unrelated proteins. *ACS Chem. Biol.* **10**, 2772–2784 (2015).
50. Akuzawa, N., Obinata, H., Izumi, T. & Takeda, S. Morphine is an exogenous ligand for MrgX2, a G-protein-coupled receptor for cortistatin. *J. Cell Animal Biol.* **2**, 004–009 (2007).
51. Wu, H.E., Schwasinger, E.T., Terashvili, M. & Tseng, L.F. dextro-Morphine attenuates the morphine-produced conditioned place preference via the sigma(1) receptor activation in the rat. *Eur. J. Pharmacol.* **562**, 221–226 (2007).

Acknowledgments

Support was given by National Institutes of Health (NIH) grants U01104974 (B.L.R., B.K.S. and W.K.K.), the NIH Department of Pharmacology Training Grant (K.L.), a Genentech Foundation Pre-doctoral Fellowship (J.K.), and a PhRMA Foundation Predoctoral Fellowship (K.L.). We thank the National Institute on Drug Abuse Drug Supply Program for supplying the morphine and codeine analogs and the glucuronidated or acetylated metabolites used in this study.

Author contributions

K.L. performed the *in vitro* pharmacology and molecular biology and wrote the paper. J.K. designed and developed homology models, carried out docking screens, analyzed results, and wrote the paper. J.L. synthesized the probe enantiomers. X.-P.H. performed GPCRome screening and assisted with *in vitro* pharmacology experiments. J.D.M. performed binding studies and *in vitro* pharmacology. W.K.K. assisted in the *in vitro* small-molecule screening and helped with data and statistical analyses. T.C. performed *in vitro* pharmacology experiments. H.N. synthesized (+)-TAN-67 and KNT-127. F.I.C. synthesized several compounds and advised structure–activity relationship studies. J.J. supervised chemical synthesis of probe enantiomers. B.L.R. and B.K.S. coordinated and supervised the project, and with the other authors wrote the paper.

Competing financial interests

The authors declare no competing financial interests.

Additional information

Any supplementary information, chemical compound information and source data are available in the online version of the paper. Reprints and permissions information is available online at http://www.nature.com/reprints/index.html. Correspondence and requests for materials should be addressed to B.L.R.

ONLINE METHODS

Cell lines. HTLA cells were a gift from R. Axel (Columbia University) and were maintained at low passage batches. FLP-IN/T-REX HEK-293-T cells were purchased from Invitrogen for ease of inducible stable cell line generation and were certified as HEK-T and mycoplasma-free by Invitrogen. FLP-IN/T-REX cells were made into inducible stable cell lines according to the manufacturer's instruction. The LAD2 human mast cell line was obtained from cells' original source lab of A. Kirshenbaum and D. Metcalfe[52] at the Laboratory of Infectious Diseases at the National Institutes of Health in Bethesda, Maryland and were maintained as per the instructions. No further characterization of HTLA or LAD2 cells was performed, as the cells came from the source labs.

Chemical compounds. The nine libraries used in screening were the NCC-1 (NIH Clinical Collection), NCC-2 (NIH Clinical Collection), NIMH Library, Tocris, Prestwick, LOPAC, Selleck, Spectrum, and the Roth Lab Collection (in-house). Opioid ligands were obtained from either Sigma-Aldrich or were synthesized.

Constructs. MRGPRX-Tango plasmids for MRGPRX1, MRGPRX2, or MRGPRX4 were made as was previously described[6]. MRGPRB2 insert was obtained from Dharmacon cDNA and subcloned into the PRESTO-Tango backbone.

PRESTO-Tango assay screening. HTLA cells (HEK-T cells stably expressing a β-arrestin2-TEV fusion protein and a tTa-dependent luciferase reporter) were maintained in DMEM (Corning) containing 10% FBS, 2 μg/ml puromycin and 100 μg/ml hygromycin B in a humidified atmosphere at 37 °C with 5% CO_2. In brief, cells were plated to 50% confluency and transfected with a codon-optimized MRGPRX-Tango construct using the calcium phosphate method[53]. The next day, transfected cells were transferred to glass-bottomed, poly-L-lysine-coated white 384-well plates at a density of 20,000 cells/well. The following day, cells were treated with 10 μM concentrations of small molecules (in quadruplicate) diluted in drug buffer (1× HBSS with 20 mM HEPES and 0.3% bovine serum albumin, pH 7.4) and incubated for 18–24 h. After drug incubation, medium was removed and 20 μl of Bright-Glo (Promega; diluted 20-fold) was added to each well and incubated 15 min at room temperature. Luminescence was measured on a TriLux luminescence counter and analyzed as relative luminescent units (RLU) using GraphPad Prism. Compounds that increased the luminescence signal by two-fold or greater were considered 'actives' and were analyzed further using concentration–response curves. More detailed discussion of the PRESTO-Tango assay can be found in ref. 6. Total number of dose–response replicates for each compound can be found in **Supplementary Table 2**. Screening metrics and detailed information related to the screening procedure can be found in **Supplementary Table 3**.

Intracellular calcium mobilization assay. We generated a MRGPRX2-expressing tetracycline-inducible stable cell line containing the MRGPRX2 codon-optimized receptor sequence with a N-terminal FLAG tag using the FLP-IN/T-REX Core Kit (Invitrogen) following the manufacturer's instructions. MRGPRX2 stable cells were maintained in DMEM containing 10% FBS, 100 μg/ml hygromycin B, and 15 μg/ml blasticidin. For the calcium mobilization assay, cells were plated into glass bottomed, poly-L-lysine coated, black 384 well plates at a density of 20,000 cells/well in medium containing 1% dialyzed FBS, 1 μg/ml tetracycline, 100 IU/ml penicillin and 100 μg/ml streptomycin and incubated 24 h. Following tetracycline induction, medium was removed and cells were loaded with 20 μl/well of 1× FLIPR Calcium dye (Molecular Devices) and 2.5 mM probenic acid, for 1 h in a humidified environment at 37 °C with 5% CO_2. For mast cell calcium experiments, cells were seeded at a density of 50,000 cells/well in Tyrode's buffer containing 1× calcium dye and incubated for 1 h before treatment and analysis. After dye loading, baseline was measured for 10 s before drug treatment, and then cells were treated with 10 μl of 3× concentrated drug in drug buffer (1× HBSS with 20 mM HEPES and 2.5 mM probenic acid, pH 7.4) in 16 point concentration response curves from 100 μM to 0.003 nM. Fluorescence was measured for an additional 120 s and data was analyzed using GraphPad Prism. Total number of dose–response replicates for each compound can be found in **Supplementary Table 2**.

β-hexosaminidase assay. LAD2 cells were maintained in Stem-Pro34 medium (GIBCO) supplemented with StemPro34 Supplement (GIBCO), 2 mM L-Glutamine, 100 U/ml penicillin–streptomycin, and recombinant human stem cell factor (100 ng/ml) (PeproTech) as described in ref. 52. For the assay, adapted from ref. 54, cells were incubated in fresh medium for 18 h before the experiment. For testing IgE activation, cells were also incubated with biotin-labeled IgE during this time. Then, cells were washed twice in Tyrode's buffer (20 mM HEPES with 134 mM NaCl, 5 mM KCl, 1.8 mM $CaCl_2$, 1 mM $MgCl_2$, 5.5 mM glucose, and 0.3% bovine serum albumin, pH 7.4) and seeded at 10,000 cells per well in V-bottom clear 96-well plates in 90 μl of Tyrode's buffer. Drugs were diluted at single concentrations or in 8-point concentration–response curves at a 10× working concentration in Tyrode's buffer and 10 μl drug, or streptavidin for biotin-labeled IgE samples, and were added in triplicate to the 90-μl mast cell suspension. Drugs and cells were incubated for 30 min in a humidified incubator without CO_2 at 37 °C. After drug incubation, plates were centrifuged at 250*g* for 5 min, and 30 μl supernatant was added to new 96-well plates containing 10 μl of 10 μM 4-nitrophenyl *N*-acetyl-β-D-glucosaminide (NAG) diluted in 0.1 M citrate buffer (49.5% 0.1M citric acid and 50.5% 0.1M sodium citrate, pH 4.5). The remaining supernatant was discarded, and cells were lysed by adding 100 μl of Tyrode's buffer with 0.1% Triton-X-100 to the pellets and mixing. 30 μl of lysate was added to 10 μl of 10 μM NAG. All plates were incubated for 90 min in a humidified incubator without CO_2 at 37 °C. Lastly, 100 μl of bicarbonate buffer (88 mM $Na2CO_3$, 40 mM $NaHCO_3$, pH 10) was added to stop the reaction, inducing a color change that was measured on an absorbance plate reader (BMG Labtech POLARstar Omega) at 405 nm. Results were analyzed by dividing the released fraction by the total fraction (released + lysed) and multiplying by 100 to get a percentage of degranulation. To correct for spontaneous degranulation, average percent degranulation for DMSO-treated wells was subtracted from drug-treated wells. Total number of dose–response replicates for each compound is reflected in figures and figure legends.

Short interfering RNA (siRNA) knockdown and qPCR analysis. Using TransIT 20/20 transfection reagent (Mirus), 25 nM of each siRNA (Dharmacon #EQ-005666-00-0002, set of four distinct MRGPRX2 siRNAs) or the nontargeting siRNA control (Dharmacon #D-001910-10-05) was prepared in 250 μl of OPTI-MEM with 5 μl TransIT per reaction. After 30 min, the transfection mixture was added drop-wise to 1.2 million mast cells/well of a 6-well plate and allowed to incubate for 72 h. After 72 h, 200,000 cells were removed for use in the β-hexosaminidase assay and 1 million cells were assayed using qRT-PCR analysis with the High-Capacity cDNA Reverse Transcription Kit (Life Technologies) following the manufacturer's instructions as well as TaqMan Universal Master Mix II with UNG (Life Technologies) and TaqMan Gene Expression Assay for MRGPRX2 (Life Technologies #4331182, Hs00365019_s1) following the manufacturer's suggested protocol.

Significance calculations of siRNA experiments. To assess significance, we used GraphPad Prism to perform a two-way ANOVA and Sidak post hoc with an alpha value of 0.05. Total number of replicates is reflected in figure legends and figures.

Homology modeling. The alignment for the construction of the MRGPRX2 models was generated using PROMALS3D[55], and homology models were built with MODELLER-9v8 (ref. 28) using the crystal structure of the κ-opioid receptor (PDB code 4DJH) as the template. The homology models were aligned against the entire MRGPRX and opioid receptor family. The alignment was manually edited to remove the amino and carboxy termini that extended past the template structure, to remove the engineered T4 lysozyme, and to create different alignments of the flexible and nonconserved second extracellular loop (EL2); the final resulting sequence alignment between the template opioid structure and the MRGPRX receptors is shown in **Supplementary Figure 5c**. Three models were built from each of 180 elastic network models (ENMs), produced by the program 3K-ENM[29], for a total of 540 models built during each iterative round of model refinement. Although EL2 is substantially shorter in MRGPRX2 than in other GPCRs, and it lacks the conserved disulfide bond between TM3 and EL2, an additional 540 models were also built forcing a putative disulfide between Cys168 in EL2 and Cys180 in TM5.

Model evaluation. Models were ranked on the basis of prioritizing active opioids (dextromethorphan) over the rest of the inactive PRESTO-Tango library that was used in the β-arrestin screen, as well as over property-matched decoy small molecules. We further insisted that in its docked pose, dextromethorphan engaged in an ion pair between its charged nitrogen and an anionic side chain in MRGPRX2. The entire PRESTO-Tango library was docked to an analogous 4DJH ligand-binding site in the modeled MRGPRX2 receptors for several rounds of iterative binding site refinement. In each round, the top-ranked models were examined for a binding pose that made hydrophobic and electrostatic interactions with the receptor, including the key positive–negative charge coordination. Residues within 6 Å of the dextromethorphan pose were then minimized around the docked ligand with PLOP[56]. The PRESTO-Tango library was then redocked into this optimized binding site for each model. This refinement continued for several cycles until the top-ranked models all converged to the same dextromethorphan pose, with the top-scoring model chosen as the final one. Structural models (PDB files) of characteristic MRGPRX2-modeled complexes (with dextromethorphan and ZINC-9232) are shown in **Supplementary Data Sets 1** and **2**.

Virtual screens. We used DOCK 3.6 to screen the ZINC database (http://zinc15.docking.org/) (Results). The flexible ligand sampling algorithm in DOCK 3.6 superimposes atoms of the docked molecule onto binding site matching spheres, which represent favorable positions for individual ligand atoms. Forty-five matching spheres were used, with each respectively starting from the previous refinement round's best pose of dextromethorphan. The degree of ligand sampling is determined by the bin size, bin-size overlap, and distance tolerance, set at 0.4 Å, 0.1 Å and 1.5 Å, respectively, for both the matching spheres and the docked molecules. The complementarity of each ligand pose was scored as the sum of the receptor–ligand electrostatic and van der Waals' interaction energies and corrected for context-dependent ligand desolvation using QNIFFT point-charge Poisson-Boltzmann electrostatics models[57]. Partial charges from the united-atom AMBER[58] force field were used for all receptor atoms; ligand charges and initial solvation energies were calculated using AMSOL[59,60] (http://comp.chem.umn.edu/amsol/). The best scoring conformation of each docked molecule was then subjected to 100 steps of rigid-body minimization.

Selection of potential ligands for testing. We docked the approximately 3.7 million commercially available molecules of the lead-like subset of the ZINC database to the final MRGPRX2 models. The full hit list was automatically filtered to remove molecules that possess high internal energy, nonphysical conformations, which are not well modeled by our scoring function. The reported rankings reflect this filtering. From the top 0.13% (~5,000 molecules) of the docked ranking list, 20 compounds were chosen for testing, based on complementarity to the binding site and presence of predicted charge interactions with Glu164$^{4.60}$ and Asp184$^{5.38}$, mimicking those predicted for dextromethorphan.

Chemistry general procedures. HPLC spectra for all compounds were acquired using an Agilent 1200 Series system with DAD detector. Chromatography was performed on a 2.1 × 150 mm Zorbax 300SB-C_{18} 5 µm column with water containing 0.1% formic acid as solvent A and acetonitrile containing 0.1% formic acid as solvent B at a flow rate of 0.4 ml/min. The gradient program was as follows: 1% B (0–1 min), 1–99% B (1–4 min), and 99% B (4–8 min). High-resolution mass spectra (HRMS) data were acquired in positive ion mode using an Agilent G1969A API-TOF with an electrospray ionization (ESI) source. Nuclear magnetic resonance (NMR) spectra were acquired with a Bruker DRX-600 spectrometer (600 MHz ^{1}H, 150 MHz ^{13}C). Chemical shifts are reported in p.p.m. (δ). HPLC was used to establish the purity of target compounds. All final compounds had > 95% purity using the HPLC methods described above.

7-Chloro-5-phenylpyrazolo[1,5-a]pyrimidine. The title compound was synthesized according to a known literature procedure[61]. To a solution of 3-aminopyrazole (2.0 g, 24 mmol) in acetic acid (15 ml) was added ethylbenzoylacetate (4.7 ml, 27 mmol). The resulting reaction mixture was refluxed for 3 h before being cooled to room temperature and concentrated. The solid residue was diluted with EtOAc and filtered to afford 5-phenylpyrazolo[1,5-*a*]pyrimidin-7(4*H*)-one (4.19 g, 83%) as white solid. This intermediate (1.0 g, 4.7 mmol) was dissolved in $POCl_3$ (5.0 ml, 55 mmol). To the resulting solution was added pyridine (0.25 ml, 3.1 mmol) at room temperature. After being stirred for 3 d at room temperature, the reaction mixture was diluted with Et_2O (50 ml) and filtered. The solid was rinsed with Et_2O (2×). The combined Et_2O solution was cooled to 0 °C and treated with ice and water. The organic layer was washed with water (2×) and brine (2×). The organic layer was dried (Na_2SO_4) and concentrated to give the tittle compound (0.82 g, 76%) as pale yellow solid. ^{1}H NMR (600 MHz, $CDCl_3$) δ 8.23 (d, *J* = 2.3 Hz, 1H), 8.12 – 8.04 (m, 2H), 7.58 – 7.48 (m, 3H), 7.45 (s, 1H), 6.84 (d, *J* = 2.3 Hz, 1H). ^{13}C NMR (151 MHz, $CDCl_3$) δ 156.2, 149.8, 146.1, 139.2, 136.5, 131.0, 129.2 (2C), 127.5 (2C), 105.8, 98.8. HRMS (ESI–TOF) *m/z*: $[M+H]^+$ calculated for $C_{12}H_9ClN_3$, 230.0485; found: 230.0484.

(R)-N,N-Dimethyl-1-(5-phenylpyrazolo[1,5-a]pyrimidin-7-yl)pyrrolidin-3-amine ((R)-ZINC-3573). To a solution of 7-chloro-5-phenylpyrazolo[1,5-*a*]pyrimidine (0.069 g, 0.3 mmol) in dioxane (2 ml) was added DIEA (0.19 ml, 0.6 mmol), followed by (*R*)-(+)-3-(dimethylamino)pyrrolidine (0.038 g, 0.33 mmol). The resulting solution was stirred for 16 h at room temperature before being concentrated and purified by silica gel column to provide the title compound (0.070 g, 76%). ^{1}H NMR (600 MHz, $CDCl_3$) δ 8.02 – 7.97 (m, 2H), 7.95 (d, *J* = 2.3 Hz, 1H), 7.51 – 7.40 (m, 3H), 6.48 (d, *J* = 2.3 Hz, 1H), 6.12 (s, 1H), 4.30 (t, *J* = 8.8 Hz, 1H), 4.23 (t, *J* = 9.8 Hz, 1H), 4.02 (q, *J* = 9.4 Hz, 1H), 3.83 (t, *J* = 9.5 Hz, 1H), 2.90 – 2.82 (m, 1H), 2.36 (s, 6H), 2.29 – 2.21 (m, 1H), 2.01 – 1.91 (m, 1H). ^{13}C NMR (151 MHz, $CDCl_3$) δ 157.5, 151.8, 147.9, 143.8, 139.2, 129.6, 128.7 (2C), 127.3 (2C), 94.9, 86.2, 65.2, 55.0, 50.1, 44.5 (2C), 30.1. HRMS (ESI-TOF) *m/z*: $[M+H]^+$ calculated for $C_{18}H_{22}N_5$, 308.1875; found: 308.1871.

(S)-N,N-Dimethyl-1-(5-phenylpyrazolo[1,5-a]pyrimidin-7-yl)pyrrolidin-3-amine ((S)-ZINC-3573). The title compound (0.075 g, 81%) was prepared using the same synthetic procedure for the preparation of (*R*)-ZINC-3573 with (*S*)-(+)-3-(dimethylamino)pyrrolidine (0.038 g, 0.33 mmol). ^{1}H NMR (600 MHz, $CDCl_3$) δ 8.05 – 7.97 (m, 2H), 7.95 (d, *J* = 2.3 Hz, 1H), 7.52 – 7.39 (m, 3H), 6.48 (d, *J* = 2.3 Hz, 1H), 6.12 (s, 1H), 4.30 (t, *J* = 8.8 Hz, 1H), 4.23 (t, *J* = 9.8 Hz, 1H), 4.02 (q, *J* = 9.3 Hz, 1H), 3.83 (t, *J* = 9.5 Hz, 1H), 2.91 – 2.81 (m, 1H), 2.36 (s, 6H), 2.30 – 2.21 (m, 1H), 2.02 – 1.91 (m, 1H). ^{13}C NMR (151 MHz, $CDCl_3$) δ 157.5, 151.8, 147.9, 143.8, 139.2, 129.6, 128.7 (2C), 127.3 (2C), 94.9, 86.2, 65.2, 55.0, 50.1, 44.5 (2C), 30.1. HRMS (ESI–TOF) *m/z*: $[M+H]^+$ calculated for $C_{18}H_{22}N_5$, 308.1875; found: 308.1872.

Code availability. The DOCK3.6 program[30,36] is freely accessible to academic labs at http://dock.compbio.ucsf.edu/DOCK3.6/ or http://blaster.docking.org/ for open access use.

Data availability. The generated and analyzed raw data sets that support the findings of this study are available from the corresponding author upon reasonable request.

52. Kirshenbaum, A.S. *et al.* Characterization of novel stem cell factor responsive human mast cell lines LAD 1 and 2 established from a patient with mast cell sarcoma/leukemia; activation following aggregation of FcepsilonRI or FcgammaRI. *Leuk. Res.* **27**, 677–682 (2003).
53. Jordan, M., Schallhorn, A. & Wurm, F.M. Transfecting mammalian cells: optimization of critical parameters affecting calcium-phosphate precipitate formation. *Nucleic Acids Res.* **24**, 596–601 (1996).
54. Staats, H.F. *et al.* A mast cell degranulation screening assay for the identification of novel mast cell activating agents. *MedChemComm* **4**, 88–94 (2013).
55. Pei, J., Kim, B.H. & Grishin, N.V. PROMALS3D: a tool for multiple protein sequence and structure alignments. *Nucleic Acids Res.* **36**, 2295–2300 (2008).
56. Jacobson, M.P. Epilepsy in aging populations. *Curr. Treat. Options Neurol.* **4**, 19–30 (2002).
57. Sharp, K.A. Polyelectrolyte electrostatics: salt dependence, entropic, and enthalpic contributions to free energy in the nonlinear Poisson–Boltzmann model. *Biopolymers* **36**, 227–243 (1995).
58. Meng, E.C., Shoichet, B.K. & Kuntz, I.D. Automated docking with grid-based energy evaluation. *J. Comput. Chem.* **13**, 505–524 (1992).
59. Li, J., Zhu, T., Cramer, C.J. & Truhlar, D.G. New class IV charge model for extracting accurate partial charges from wave functions. *J. Phys. Chem. A* **102**, 1820–1831 (1998).
60. Chambers, C.C., Hawkins, G.D., Cramer, C.J. & Truhlar, D.G. Model for aqueous solvation based on class IV atomic charges and first solvation shell effects. *J. Phys. Chem.* **100**, 16385–16398 (1996).
61. Paruch, K. *et al.* Discovery of Dinaciclib (SCH 727965): a potent and selective inhibitor of cyclin-dependent kinases. *ACS Med. Chem. Lett.* **1**, 204–208 (2010).

doi:10.1038/nchembio.2334